dementia,[26] the very small number of neuropathological reports of patients with BPD[25,27] prevent any definitive conclusions.

We could not determine the effect of lithium carbonate on the neurodegenerative outcome, partly due to the small number of cases as well as the retrospective manner of our study design. Studies that are currently in progress include positron emission tomography imaging for amyloid and tau as well as alpha-synuclein imaging. Although the CSF biomarkers utilized in the diagnosis of Alzheimer's disease may be difficult to apply to BPD, our study indicates that BPD could be a potential target for these imaging studies.

ACKNOWLEDGMENTS

The authors thank Mr. Nobuo Kuninaka, Ms. Yoko Tanaka, Mr. Naoo Aikyo, Ms. Mieko Harada, Ms. Yuki Kimura and Ms. Nobuko Naoi for technical support. This study was supported by Grants-in-Aid from the Japanese Bureau of Health, Labor, and Welfare (Y.S. & S.M.) and the Ministry of Education, Science, and Technology (Y.S. & S.M.), Health and Labour Sciences Research Grant, "Research on Applying Health Technology," from the Japanese Ministry of Health, Labor and Welfare (Y.S. & S.M.) and by an Intramural Research Grant (25-7) for Neurological and Psychiatric Disorders of NCNP (Y.S.).

REFERENCES

1. Townsend J, Altshuler LL. Emotion processing and regulation in bipolar disorder: a review. *Bipolar Disord* 2012; **14**: 326–339.
2. Kato T. Molecular genetics of bipolar disorder and depression. *Psychiatry Clin Neurosci* 2007; **61**: 3–19.
3. Belmaker RH. Bipolar disorder. *N Engl J Med* 2004; **351**: 476–486.
4. Klein PS, Melton DA. A molecular mechanism for the effect of lithium on development. *Proc Natl Acad Sci U S A* 1996; **93**: 8455–8459.
5. Massot O, Rousselle JC, Fillion MP, Januel D, Plantefol M, Fillion G. 5-HT1B receptors: a novel target for lithium. Possible involvement in mood disorders. *Neuropsychopharmacology* 1999; **21**: 530–541.
6. Dixon JF, Hokin LE. Lithium acutely inhibits and chronically up-regulates and stabilizes glutamate uptake by presynaptic nerve endings in mouse cerebral cortex. *Proc Natl Acad Sci U S A* 1998; **95**: 8363–8368.
7. Manji HK, Moore GJ, Chen G. Lithium at 50: have the neuroprotective effects of this unique cation been overlooked? *Biol Psychiatry* 1999; **46**: 929–940.
8. Shimada K, Motoi Y, Ishiguro K *et al.* Long-term oral lithium treatment attenuates motor disturbance in tauopathy model mice: implications of autophagy promotion. *Neurobiol Dis* 2012; **46**: 101–108.
9. Prickaerts J, Moechars D, Cryns K *et al.* Transgenic mice overexpressing glycogen synthase kinase 3beta: a putative model of hyperactivity and mania. *J Neurosci* 2006; **26**: 9022–9029.
10. Dokucu ME, Yu L, Taghert PH. Lithium- and valproate-induced alterations in circadian locomotor behavior in Drosophila. *Neuropsychopharmacology* 2005; **30**: 2216–2224.
11. Hong M, Chen DC, Klein PS, Lee VM. Lithium reduces tau phosphorylation by inhibition of glycogen synthase kinase-3. *J Biol Chem* 1997; **272**: 25326–25332.
12. Braak H, Braak E. Argyrophilic grains: characteristic pathology of cerebral cortex in cases of adult onset dementia without Alzheimer changes. *Neurosci Lett* 1987; **76**: 124–127.
13. Tolnay M, Spillantini MG, Goedert M, Ulrich J, Langui D, Probst A. Argyrophilic grain disease: widespread hyperphosphorylation of tau protein in limbic neurons. *Acta neuropathologica* 1997; **93**: 477–484.
14. Togo T, Sahara N, Yen SH *et al.* Argyrophilic grain disease is a sporadic 4-repeat tauopathy. *J Neuropathol Exp Neurol* 2002; **61**: 547–556.
15. Ikeda K, Akiyama H, Arai T, Matsushita M, Tsuchiya K, Miyazaki H. Clinical aspects of argyrophilic grain disease. *Clin Neuropathol* 2000; **19**: 278–284.
16. McKee AC, Stern RA, Nowinski CJ *et al.* The spectrum of disease in chronic traumatic encephalopathy. *Brain* 2013; **136**: 43–64.
17. Saito Y, Ruberu NN, Sawabe M *et al.* Staging of argyrophilic grains: an age-associated tauopathy. *J Neuropathol Exp Neurol* 2004; **63**: 911–918.
18. Folstein MF, Folstein SE, McHugh PR. "Mini-mental state". A practical method for grading the cognitive state of patients for the clinician. *J Psychiatr Res* 1975; **12**: 189–198.
19. Fumimura Y, Ikemura M, Saito Y *et al.* Analysis of the adrenal gland is useful for evaluating pathology of the peripheral autonomic nervous system in lewy body disease. *J Neuropathol Exp Neurol* 2007; **66**: 354–362.
20. Saito Y, Kawashima A, Ruberu NN *et al.* Accumulation of phosphorylated alpha-synuclein in aging human brain. *J Neuropathol Exp Neurol* 2003; **62**: 644–654.
21. Braak H, Braak E. Neuropathological stageing of Alzheimer-related changes. *Acta neuropathologica* 1991; **82**: 239–259.
22. McKeith IG, Dickson DW, Lowe J *et al.* Diagnosis and management of dementia with Lewy bodies: third report of the DLB Consortium. *Neurology* 2005; **65**: 1863–1872.
23. Hatsuta H, Saito Y, Sawabe M, Mori H, Murayama S. Staging of amyloid angiopathy in human aging brain. *Neuropathology* 2007; **27**: 191.

24. Dickson DW, Bergeron C, Chin SS *et al.* Office of Rare Diseases neuropathologic criteria for corticobasal degeneration. *J Neuropathol Exp Neurol* 2002; **61**: 935–946.
25. Nagao S, Yokota O, Ikeda C *et al.* Argyrophilic grain disease as a neurodegenerative substrate in late-onset schizophrenia and delusional disorders. *Eur Arch Psychiatry Clin Neurosci* 2014; **264**: 317–331.
26. Kosaka K, Yoshimura M, Ikeda K, Budka H. Diffuse type of Lewy body disease: progressive dementia with abundant cortical Lewy bodies and senile changes of varying degree–a new disease? *Clin Neuropathol* 1984; **3**: 185–192.
27. Jellinger KA. Lewy body/alpha-synucleinopathy in schizophrenia and depression: a preliminary neuropathological study. *Acta Neuropathologica* 2009; **117**: 423–427.

ANNALS of Clinical and Translational Neurology
Open Access
RESEARCH ARTICLE

Heterozygous *Polg* mutation causes motor dysfunction due to mtDNA deletions

Satoshi Fuke[1,2], Mizue Kametani[1], Kazuyuki Yamada[3], Takaoki Kasahara[1], Mie Kubota-Sakashita[1], Gregory C. Kujoth[4], Tomas A. Prolla[5], Seiji Hitoshi[2] & Tadafumi Kato[1]

[1]Laboratory for Molecular Dynamics of Mental Disorders, RIKEN Brain Science Institute, Wako, Saitama, Japan, 351-0198
[2]Department of Integrative Physiology, Shiga University of Medical Science, Otsu, Shiga, Japan, 520-2192
[3]Research Resources Center, RIKEN Brain Science Institute, Wako, Saitama, Japan, 351-0198
[4]Department of Neurological Surgery, University of Wisconsin, Madison, Wisconsin, 53792
[5]Departments of Genetics and Medical Genetics, University of Wisconsin, Madison, Wisconsin, 53706

Correspondence
Tadafumi Kato, Laboratory for Molecular Dynamics of Mental Disorders, RIKEN Brain Science Institute, 2-1 Hirosawa, Wako, Saitama, Japan, 351-0198. Tel: +81-48-467-6949; Fax: +81-48-467-6947; E-mail: kato@brain.riken.jp

Funding Information
This work was supported by grants for the Laboratory for Molecular Dynamics of Mental Disorders, RIKEN Brain Science Institute (BSI), a Grant-in-Aid from the Japanese Ministry of Health and Labor, and Grants-in-Aid from the Japanese Ministry of Education, Culture, Sports, Science and Technology. S. F. is supported by Grants-in-Aid for young scientists from the Japanese Ministry of Education, Culture, Sports, Science and Technology, and Grants-in-Aid for young scientists from Shiga University of Medical Science.

Received: 25 June 2014; Revised: 25 September 2014; Accepted: 25 September 2014

Annals of Clinical and Translational Neurology **2014; 1(11): 909–920**

doi: 10.1002/acn3.133

Abstract

Objective: Mutations in nuclear-encoded mitochondrial DNA (mtDNA) polymerase (*POLG*) are known to cause autosomal dominant chronic progressive external ophthalmoplegia (adCPEO) with accumulation of multiple mtDNA deletions in muscles. However, no animal model with a heterozygous Polg mutation representing mtDNA impairment and symptoms of CPEO has been established. To understand the pathogenic mechanism of CPEO, it is important to determine the age dependency and tissue specificity of mtDNA impairment resulting from a heterozygous mutation in the *Polg* gene in an animal model. **Methods:** We assessed behavioral phenotypes, tissue-specific accumulation of mtDNA deletions, and its age dependency in heterozygous $Polg^{D257A}$ knock-in mice carrying a proofreading-deficient mutation in the *Polg*. **Results:** Heterozygous $Polg^{D257A}$ knock-in mice exhibited motor dysfunction in a rotarod test. $Polg^{+/D257A}$ mice had significant accumulation of multiple mtDNA deletions, but did not show significant accumulation of point mutations or mtDNA depletion in the brain. While mtDNA deletions increased in an age-dependent manner regardless of the tissue even in $Polg^{+/+}$ mice, the age-dependent accumulation of mtDNA deletions was enhanced in muscles and in the brain of $Polg^{+/D257A}$ mice. **Interpretation:** Heterozygous $Polg^{D257A}$ knock-in mice showed tissue-specific, age-dependent accumulation of multiple mtDNA deletions in muscles and the brain which was likely to result in neuromuscular symptoms. $Polg^{+/D257A}$ mice may be used as an animal model of adCPEO associated with impaired mtDNA maintenance.

Introduction

Chronic progressive external ophthalmoplegia (CPEO) is a mitochondrial neuromuscular disease presenting progressive external ophthalmoplegia and other neuromuscular symptoms. On the molecular level, the accumulation of multiple mtDNA deletions in muscles is characteristic of CPEO, which is distinct from other inherited mitochondrial diseases because of point mutations or copy number reduction of mtDNA in affected tissues.[1–3] CPEO is a relatively late-onset disease accompanied by neurological symptoms such as ataxia, exercise intolerance, fatigue, optic atrophy, cognitive impairment, and mood disorders.[4–18] Postmortem brain analyses showed increased accumulation of multiple mtDNA deletions in the brain.[4,7] Thus, neurological symptoms in CPEO likely result from the accumulation of multiple mtDNA deletions in the brain.

Mutations in nuclear-encoded proteins involved in mtDNA maintenance cause inherited CPEO.[3,8–11,18–21] The nuclear gene encoding the catalytic subunit of the mtDNA polymerase, known as DNA polymerase γ (Polg), plays a prominent role in replication and repair, which are essential for mtDNA synthesis.[14] Heterozygous mutations in *POLG* cause autosomal dominant CPEO. Thus, a heterozygous mutant *Polg* knock-in mouse may be an appropriate animal model for CPEO. Homozygous knock-in mice that carry proofreading-deficient Polg ($Polg^{D257A}$) exhibited marked accumulation of mtDNA point mutations and showed systemic physical abnormalities and reduced life span; these mice have been proposed to be an animal model of premature aging.[22–27] However, heterozygous $Polg^{D257A}$ mice were reportedly normal.[22–30]

In this study, we examined heterozygous $Polg^{D257A}$ mice in detail. These mice exhibited motor dysfunction and accumulation of mtDNA deletions in the brain and muscles in an age-dependent and tissue-specific manner.

Materials and Methods

Animals and behavioral analysis

The $Polg^{D257A}$ mouse was described previously.[23] In this study, $Polg^{+/D257A}$ mice were backcrossed for more than six generations into C57BL/6JJcl; next, selective breeding using 104 microsatellite markers covering the entire genome enabled the production of mutant mice with a genetic background similar to C57BL/6J for >99% of offspring by mating male $Polg^{+/D257A}$ mice with female C57BL/6JJcl mice purchased from CLEA Japan (Tokyo, Japan). We examined 34 weeks old male mice kept in cages with a running wheel for 7 weeks from 19 to 25 weeks. The details of a conventional behavioral test battery are described in Data S1. All animal experiments were performed in accordance with the protocols that had been approved by the Animal Experiment Committee of RIKEN (Wako, Saitama, Japan) and Shiga University of Medical Science (Otsu, Shiga, Japan). The number of animals used their suffering was minimized as much as possible.

Analysis of mtDNA point mutation

mtDNAs were purified from mice frontal lobe using the mtDNA Extractor CT kit (Wako Pure Chemical Industries, Osaka, Japan), which is based on the alkaline-SDS method for the plasmid DNA purification followed by removal of sodium iodide and RNA by RNaseA treatment. The 1782-bp fragment (#13557–15340) of mtDNA (NC_005089) from each genotype ($n = 3$) was digested using the restriction endonucleases *Xho*I and *Bgl*II and directly cloned into pBluescript SK+ plasmid DNA without polymerase chain reaction (PCR) amplification. From each mouse tissue, more than 12 independent clones were sequenced and the average mutation frequency was examined ($Polg^{+/+}$ mice: 48 total clones, $Polg^{+/D257A}$ mice: 47 total clones, $Polg^{D257A/D257A}$ mice: 53 total clones). More than 21,000 nucleotides were analyzed from each mouse.

Southern blot analysis

Purified total mtDNA was either left undigested or digested by incubation with restriction endonuclease *Bgl*II (Takara Bio, Shiga, Japan). After electrophoresis and depurination, alkaline blotting was performed by capillary transfer.

mtDNAs were detected using the Digoxigein (DIG)-labeled DNA probe for mouse mtDNA, which was described previously.[31] The DIG-labeled DNA probes for the control region (D-loop), *ND1*, and *COX1* were synthesized using the PCR DIG Probe Synthesis Kit (Roche Diagnostics, Mannheim, Germany), and whole mtDNA probe was synthesized from Taq I-digested mouse whole mtDNA using random primers and the BcaBEST DIG labeling kit (Takara).

PCR analysis

All primer sequences are described in Table S1. For PCR, mouse mtDNA was amplified from 10 ng of purified mtDNA with the 0.2 μmol/L primers D3 and D4,[31] which face outward from the D-loop of mtDNA, using SYBR Premix Ex Taq reagent (Takara Bio) with the following protocol: 95°C for 20 sec, 55°C for 20 sec, and 72°C for 13 min (for a long-extension PCR) or 80 sec (for a short-extension PCR), 35 cycles after an initial denaturation at 95°C for 1 min. For quantitative real-time PCR (qPCR) analysis, each PCR product was separately amplified from 50 ng of total DNA or 5 ng of purified mtDNA in a 10 μL reaction using SYBR Premix Ex Taq reagent. For deleted mtDNA molecules, qPCR was based on short-extension PCR. Accumulation of mtDNA deletions was assessed by determining the ratio to total mtDNA quantified with amplification of the D-loop using the primer pair D1 and D2. Other primer sets were designed to anneal to the *COX1* gene and the *ND4* gene for mtDNA, and the *ApoB* gene for nuclear DNA. Copy number was quantified by determining the ratio of total mtDNA to nuclear DNA. Real-time qPCR reactions were carried out in quadruplicate for all measurements. In every run, the quantities were calibrated using the standard curves with each control plasmid ($R^2 > 0.99$), as described previously.[32] Only a standard curve of mtDNA deletions was used to standardize the differences among runs and was

calculated between Ct values and the logarithm of concentration of extracted mtDNA from old $Polg^{D257A/D257A}$ mice (>60 weeks old) within the linear range (Fig. S4B, $R^2 > 0.95$).

In vivo mtDNA labeling and Southwestern blot analysis

Newly synthesized mtDNA molecules were labeled by 5-bromo-2-deoxyuridine (BrdU) treatment and detected by Southwestern blot analysis using anti-BrdU antibody. Eight-week-old, male C57BL/6J mice (CLEA Japan) were injected intraperitoneally with prewarmed 2′-Deoxyuridine, 5′-Triphosphate (dUTP) or BrdU (500 mg/kg body weight; 50 mg/mL; NACALAI TESQUE, Kyoto, Japan) dissolved in 0.1 mol/L NaOH and adjusted to neutral pH. mtDNA was sampled each hour from 0–12 h and at 24, 36, 48, 60, 72, 84, and 96 h after intraperitoneal injection. Southwestern blot analysis was developed using a method described previously.[33] mtDNA was digested by incubation with the restriction endonuclease *Eag*I (New England Biolabs, Beverly, MA) and transferred using the same method used for Southern blot analysis. After BrdU imaging with anti-BrdU antibody (Becton Dickinson Immunocytometry Systems, San Jose, CA), and an HRP-conjugated anti-mouse IgG secondary antibody (Jackson ImmunoResearch Laboratories, West Grove, PA) by Western Lightning™ Chemiluminescence Reagent (Perkin Elmer, Waltham, MA) and LAS-3000 (FUJIFILM, Tokyo, Japan), antibodies were stripped for Southern blot analysis. The relative levels of newly generated mtDNA after injection was quantified by determining the value of incorporation of BrdU into mtDNA based on the BrdU/mtDNA signal intensity ratio measured using Multi Gauge Ver 2.2 software (FUJIFILM).

Cell culture and immunofluorescence analysis

Primary neurons were isolated from mouse embryos at gestational day 17–18 and cultured as described previously.[34] To detect localization of BrdU signals in the mitochondria as an indicator of newly synthesized mtDNA, neurons were cultured in the presence 10 μmol/L BrdU for 48 h after 7 days of incubation for differentiation. Neurons were fixed and immunocytochemically stained as reported previously.[35] In some experiments, neurons were also cultured in the presence of 100 nmol/L MitoTracker Red CM-H2XRos for 1 h before fixation or were incubated with NeuroTrace Red Fluorescent Nissl Stain (Life Technologies, Carlsbad, CA) at room temperature for 20 min following the anti-BrdU staining. Images were acquired using a confocal microscope (FV1000; Olympus, Tokyo, Japan) from at least three independent culture preparation. Protocols to isolate neural stem cells and generate neurospheres from embryonic brain in vitro have been described previously.[36]

Statistical analysis

The results of quantitative experiments were analyzed by parametric or nonparametric tests after conducting a Kolmogorov–Smirnov test to confirm a normal distribution. A two-tailed test was used for all analysis. Statistical significance ($P < 0.05$) was determined using SPSS 18.0 software (SPSS, Chicago, IL) and KyPlot 4.0 (KyensLab, Tokyo, Japan).

Results

Behavioral phenotypes of $Polg^{+/D257A}$ mice

We examined 34 weeks old male mice carrying the heterozygous $Polg^{D257A}$ mutation (referred to as $Polg^{+/D257A}$) using a conventional behavioral test battery. Homozygous $Polg^{D257A}$-mutant mice (referred to as $Polg^{D257A/D257A}$ mice) were also assessed as a positive control group for mitochondrial dysfunction, apoptosis, and sarcopenia in skeletal muscle.[25,26,28] As expected, $Polg^{D257A/D257A}$ mice showed significantly lower body weight than mice of other genotypes, poor performance in the rotarod test, and reduced spontaneous motor activity in the open field test, elevated plus maze, and Y-maze test (Fig. S1). In the rotarod test, not only $Polg^{D257A/D257A}$ mice but also $Polg^{+/}$

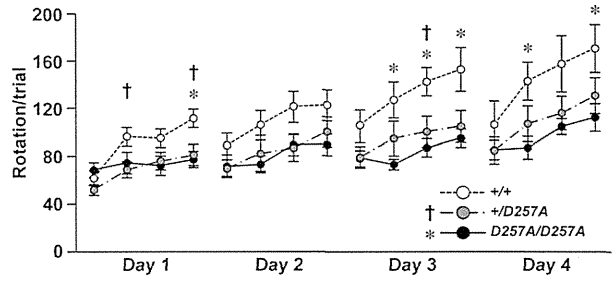

Figure 1. Rotarod test for evaluating motor function among $Polg^{+/+}$ mice ($n = 9$), $Polg^{+/D257A}$ ($n = 10$), and $Polg^{D257A/D257A}$ ($n = 10$) mice. The general linear model repeated measures ANOVA followed by Tukey's honestly significant difference (HSD) (mean rotations ± SEM) showed significant effects of genotype ($P = 0.026$) and days ($P < 1.00 \times 10^{-10}$), but no interaction between genotype and days ($P = 0.082$). $Polg^{+/D257A}$ mice generally showed lower performance than $Polg^{+/+}$ mice ($P = 0.077$), which was similar to $Polg^{D257A/D257A}$ mice ($Polg^{+/D257A}$ mice vs. $Polg^{D257A/D257A}$ mice: $P = 0.885$, $Polg^{D257A/D257A}$ mice vs. $Polg^{+/+}$ mice: $P = 0.029$). These results were supported by significant differences between $Polg^{+/+}$ and $Polg^{+/D257A}$ mice (†$P < 0.05$), or $Polg^{D257A/D257A}$ mice (*$P < 0.05$) in analysis of each trial.

^{D257A} mice showed significantly poor performance than $Polg^{+/+}$ mice for a number of trials (Fig. 1). $Polg^{+/D257A}$ mice did not differ from $Polg^{+/+}$ mice in other tests. The result indicates that the motor dysfunction caused by the heterozygous mutation in *Polg* is milder than that caused by the homozygous mutation.

Accumulation of mtDNA deletions in the brain of $Polg^{+/D257A}$ mice

The motor dysfunction in $Polg^{+/D257A}$ mice prompted us to investigate whether mtDNA was impaired by the heterozygous mutation in *Polg*. Therefore, we evaluated mtDNA alterations in the brain of $Polg^{+/D257A}$ mice. Southern blot analysis of purified mtDNA using a probe for the control region (D-loop) (Fig. 2A and B) showed the presence of small mtDNAs corresponding to deletion mutants in the frontal lobe of $Polg^{+/D257A}$ mice. These small mtDNAs were observed in the frontal lobe of $Polg^{+/D257A}$ mice at 62 weeks of age upon overexposure (Fig. 2B). However, small mtDNAs were not detectable in $Polg^{+/D257A}$ mice at 24 weeks and in $Polg^{+/+}$ mice at 62 weeks at the same experimental condition. Additionally, apparent multiple mtDNA signals were observed in $Polg^{D257A/D257A}$ mice at 62 weeks, subtle signals were observed at 24 weeks (Fig. 2A). Consistent with the results of previous studies, there was no detectable signal other than full-length mtDNA using probes for gene-encoding regions of mtDNA, even in $Polg^{D257A/D257A}$ mice (Fig. S2A). Accumulation of multiple mtDNA deletions in the frontal lobe of $Polg^{+/D257A}$ mice at 62 weeks was confirmed by PCR analyses (Fig. 2C–E). Long-range PCR amplification of mtDNA revealed the presence of variously sized mtDNA molecules with deletions in the brain of $Polg^{+/D257A}$ mice (Fig. 2C). Full-length mtDNA was observed, but there were fewer deletion molecules in $Polg^{+/+}$ mice than in $Polg^{+/D257A}$ mice. Moreover, short-extension PCR was used to selectively amplify small mtDNA molecules to clarify the difference between $Polg^{+/D257A}$ and $Polg^{+/+}$ mice (Fig. 2D). Using highly sensitive qPCR analysis (see Materials and Methods, Fig. S2B and C), significantly increased accumulation of mtDNA deletions was observed in $Polg^{+/D257A}$ mice (Fig. 2E). In frontal lobe of $Polg^{+/D257A}$ mice, there was a reduction in protein level of mtDNA-encoded subunits of Complex IV (Fig. S3).

We also investigated mtDNA point mutations in frontal lobe. $Polg^{D257A/D257A}$ mice showed significant accumulation of point mutations compared to other mice. Although $Polg^{+/D257A}$ mice also showed a similar tendency of higher number of mtDNA point mutations than $Polg^{+/+}$ mice, this difference was not statistically significant (Fig. 2F). In addition to point mutations, crucial single nucleotide insertion/deletion were found in six clones from $Polg^{D257A/D257A}$ mice. Moreover, $Polg^{D257A/D257A}$ mice showed a significantly reduced mtDNA copy number in frontal lobe, posterior cortex, basal ganglia, and cerebellum. No significant difference in mtDNA copy number was observed between $Polg^{+/+}$ and $Polg^{+/D257A}$ mice (Fig. 2G). Thus, the formation and accumulation of mtDNA deletions, but not point mutations and mtDNA depletion, were detected in $Polg^{+/D257A}$ mice.

Age-dependent increase in mtDNA deletions is accelerated in muscle and the brain of $Polg^{+/D257A}$ mice

We investigated mtDNA deletion levels in detail in the brain, which was divided into five areas (frontal lobe, posterior cortex, cerebral cortex except for the frontal lobe, hippocampus, basal ganglia, cerebellum), and in other somatic tissues (heart, liver, kidney, and skeletal muscles) of $Polg^{+/+}$ and $Polg^{+/D257A}$ mice at 48 weeks of age. Deletions in the heart were clearly detected in all $Polg^{+/D257A}$ mice by Southern blot analysis (Fig. 3A, upper panel). Deleted mtDNA signals in the frontal lobe, posterior cortex, and hippocampus of $Polg^{+/D257A}$ mice were detectable after overexposure in Southern blot analysis, same as is shown in Figure 2B, but were not detectable at all in $Polg^{+/+}$ mice (Fig. 3A, lower panel). Consistent with the results of Southern blot analysis, significant differences were verified by short-extension qPCR analysis in the frontal lobe, posterior cortex, and hippocampus, and heart, but not in the cerebellum, liver, kidney, and skeletal muscles at 48 weeks (Fig. 3B). On the other hand, $Polg^{D257A/D257A}$ mice indeed showed much higher levels of mtDNA deletions in all tissues we tested (Fig. S4).

To understand the effect of age on accumulation of multiple mtDNA deletions, we measured mtDNA deletion levels in each brain region, muscles, and liver in $Polg^{+/+}$ and $Polg^{+/D257A}$ mice of various ages (Figs. 3C and S5). mtDNA deletions accumulated with age in an exponential manner regardless of tissues or genotypes. However, there was a significant interaction between genotype and age; the heterozygous *Polg* mutation accelerated the age-dependent increase in mtDNA deletions in the brain and muscles, including the cerebellum and skeletal muscles, but not the liver. In contrast, mtDNA copy number was not affected by age or genotype, whereas a significant difference was found between tissues (Fig. S6). Although the increase in mtDNA deletion was not detected until 60 weeks in mtDNA analysis utilizing the entire skeletal muscle in hind limb, a part of skeletal muscle of hind limb of $Polg^{+/D257A}$ mice showed the significant enhancement of accumulation of mtDNA deletions at 37 weeks corresponding period of the rotarod test (Fig. S7).

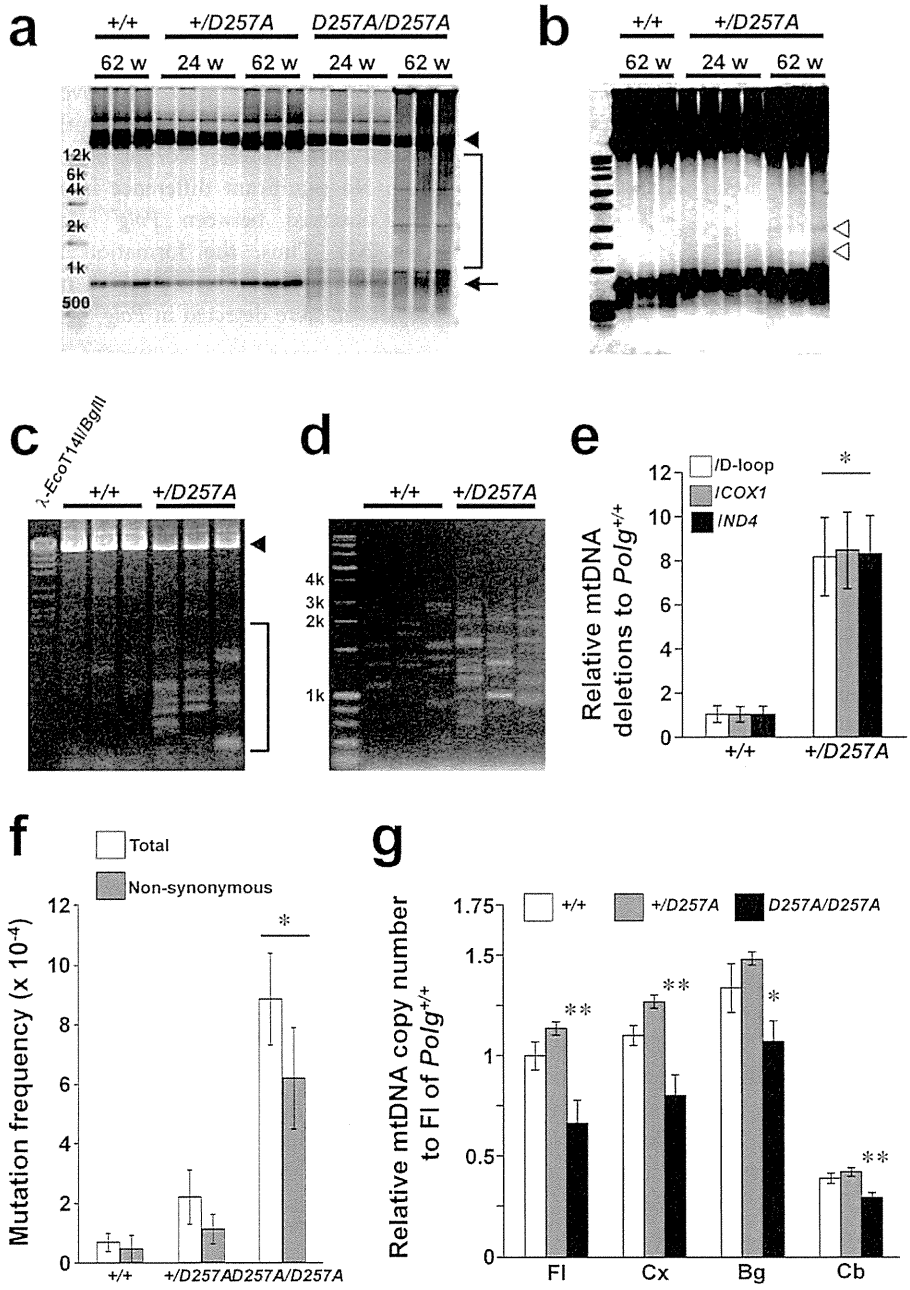

Figure 2. mtDNA analysis in the brain of mice. (A) Southern blot analysis of the frontal lobe mtDNA using a probe for the control region of mtDNA. Signals of full-length mtDNA (arrowhead), 7S DNA forming the displacement loop (D-loop; arrow), and mtDNA deletions (square bracket) can be observed. Signals for mtDNAs smaller than the full-length 16.5-kb signal were detected strongly in the frontal lobe of $Polg^{D257A/D257A}$ mice at 62 weeks and more subtly at 24 weeks. (B) Overexposed Southern blot analysis of mtDNA in the frontal lobe of $Polg^{+/+}$ and $Polg^{+/D257A}$ mice in panel A. Modest mtDNA signals (open arrowheads) were detectable in $Polg^{+/D257A}$ mice, but not in $Polg^{+/+}$ mice. (C) Long-range PCR of the frontal lobe mtDNA. Full-length mtDNA (arrow head) in all mice and deletion molecule size (square bracket) in $Polg^{+/D257A}$ mice ($n = 3$) were observed. (D) Short-extension PCR for selective amplification of deletion molecules. Amplicon-derived mtDNA deletions in the frontal lobe were more obvious in $Polg^{+/D257A}$ mice than $Polg^{+/+}$ mice. (E) Quantitative analysis of accumulation of mtDNA deletions in the frontal lobe using qPCR. Accumulation levels were determined using the D-loop (white), *COX1* (gray), or *ND4* (black) region of mtDNA as a reference ($n = 3$, mean ± SD, $^*P < 0.02$, *t*-test). (F) Quantitative analysis of mtDNA point mutation in the frontal lobe of mice at 62 weeks. Numbers of total mutations (white columns, Welch ANOVA followed by Dunnett's T3 test) and nonsynonymous mutations (gray columns, one-way ANOVA followed by Tukey's HSD) are indicated ($n = 3$, mean ± SD, $^*P < 0.025$). (G) Analysis of mtDNA copy number in the frontal lobe, posterior cortex, basal ganglia, and cerebellum of mice: $Polg^{+/+}$ mice (white columns), $Polg^{+/D257A}$ mice (gray columns), and $Polg^{D257A/D257A}$ mice (black columns). The vertical axis represents the relative value normalized to the average copy number of mtDNA in frontal lobe of $Polg^{+/+}$ mice ($n = 3$, mean ± SD, $^{**}P < 0.01$, $^*P < 0.05$, Welch ANOVA followed by the Dunnett's T3 test).

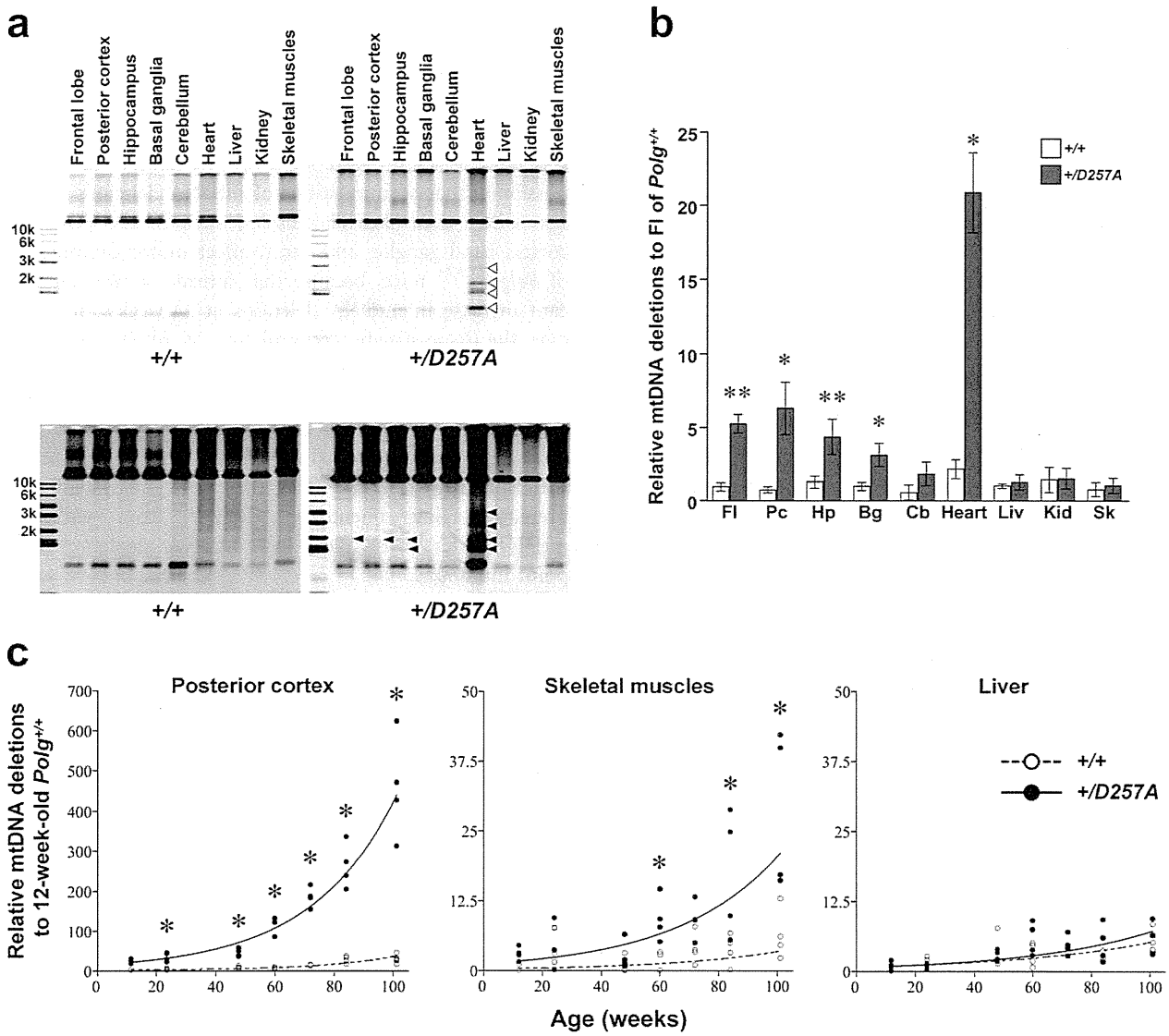

Figure 3. Tissue-specific accumulation of mtDNA deletions in *Polg*$^{+/D257A}$ mice. (A) Southern blot analysis of accumulation in tissues of *Polg*$^{+/D257A}$ and *Polg*$^{+/+}$ mice (n = 3) at 48 weeks using a probe containing D-loop, a representative result is shown. mtDNA deletions were detected in the heart of *Polg*$^{+/D257A}$ mice (open arrowheads) but not in *Polg*$^{+/+}$ mice. In *Polg*$^{+/D257A}$ mice, slight signals of deletion molecules were detectable in the frontal lobe, posterior cortex, and hippocampus of only *Polg*$^{+/D257A}$ mice after overexposure (lower panel, arrowheads). (B) qPCR analysis to compare accumulation of mtDNA deletions in the frontal lobe (Fl), posterior cortex (Pc), hippocampus (Hp), basal ganglia (Bg), cerebellum (Cb), heart, liver (Liv), kidney (Kid), and skeletal muscles (Sk) of *Polg*$^{+/D257A}$ mice with that of *Polg*$^{+/+}$ mice at 48 weeks old. Relative accumulation normalized to that in the frontal lobe of *Polg*$^{+/+}$ mice is represented (n = 3, mean ± SD, $^{**}P < 0.01$, $^{*}P < 0.05$, t-test). Significant differences were observed among tissues of *Polg*$^{+/D257A}$ mice: Fl and heart > Liv, Kid, and Sk; heart > all brain areas ($P < 0.05$, Welch ANOVA followed by the Dunnett T3 test). (C) Analysis of age-dependent accumulation of mtDNA deletions in the frontal lobe and skeletal muscles of *Polg*$^{+/D257A}$ and *Polg*$^{+/+}$ mice at 12, 24, 48, 60, 72, 84, and 101 weeks using qPCR. Values are those relative to the average of 12-week-old *Polg*$^{+/+}$ mice in each tissue. Each circle indicates one mouse (n = 4; two males and two females). Results in other brain areas, heart, and liver are shown in Figure S5. A significant effect of genotype and a significant interaction between genotype and age upon increase in mtDNA deletions was observed in the brain and muscles ($P < 0.001$, ANCOVA with a factor of genotype and a covariate of age), but not for the liver ($P > 0.2$). In ANCOVA with a factor of tissues and a covariate of age in each genotype, difference among tissues and the interaction between tissue and age were significant ($P < 0.001$). Significant differences were detected at several ages, except for in the liver ($^{*}P < 0.05$). Significant effects of age were observed in all tissues regardless of genotype ($P < 1.00 \times 10^{-5}$, ANCOVA with a factor of genotype and a covariate of age).

Furthermore, a significant decrease in complex IV (COX) activities was observed in skeletal muscles of $Polg^{+/D257A}$ mice at 96 weeks (Fig. S8) similar to that in cortex of $Polg^{+/D257A}$ mice in previous report.[37]

In neural stem cells (NSCs) cultured for 5 weeks from mouse embryos, no difference was observed between NSCs from $Polg^{+/D257A}$ mice and those from $Polg^{+/+}$ mice, although NSCs from $Polg^{D257A/D257A}$ mice accumulated mtDNA deletions (Fig. S9). These results suggest that aging plays an important role in the accumulation of mtDNA deletions in the brain of $Polg^{+/D257A}$ mice.

mtDNA replicates more rapidly in the mouse brain than in the liver

Since mtDNA deletions and point mutations were accumulated in mouse brain which contains nondividing neurons, we estimated the probability that quiescent cells are constantly metabolizing mtDNA and accumulate mtDNA mutations during mtDNA synthesis. To verify the active mtDNA synthesis, we treated primary cultured neurons from wild-type mouse embryos with BrdU for 48 h. We showed that BrdU signals were localized in the mitochondria in the cell bodies and neurites, but not in the nuclei (Fig. 4A), in postmitotic neurons.

Tissue-dependent difference in mtDNA synthesis rate may also contribute to the tissue-dependent accumulation of mtDNA deletions. Thus, we examined differences in mtDNA synthesis between the liver (Fig. 4B, D, and F) and brain (posterior cortex) (Fig. 4C, E, and G) by in vivo mtDNA labeling with BrdUin adult wild-type mice at 8 weeks of age. Incorporation of BrdU (Fig. 4B and C) into mtDNA (Fig. 4D and E) increased over time in the both tissues from an hour or two after the injection (Fig. 4F and G). A significant dependence was observed between tissues over time. The time to reach the half-maximal level of BrdU incorporation ($T_{1/2}$) was shorter in the brain (posterior cortex) (Fig. 4G and H, ~4 h) than in the liver (Fig. 4F and H, 7–8 h).

Discussion

Despite clinical studies indicating that heterozygous *POLG* mutations cause CPEO, neuromuscular symptoms and accumulation of mtDNA deletions in $Polg^{+/D257A}$ mice have not been reported. In this study, we found that a heterozygous mutation of *POLG* could cause neuromuscular symptoms similar to those found in CPEO patients. Moreover, we showed that the D257A mutation in one allele of the *Polg* gene was sufficient to cause accumulation of multiple mtDNA deletions in the brain and muscles, but accumulation of mtDNA point mutations and mtDNA copy number reduction is absent or less prominent. It is still controversial whether mtDNA point mutations are increased in the $Polg^{+/D257A}$ mice.[22,27] However, the present results suggest that mtDNA deletions are more prominent than point mutations. In addition to skeletal muscles in posterior crus, we cannot rule out a possibility that accumulations of mtDNA deletions in tissues other than skeletal muscles, such as the posterior cortex, basal ganglia, and heart, affect motor dysfunction of $Polg^{+/D257A}$ mice, because they already showed significant increase in mtDNA deletions at 24 weeks. In either case, the tissue-specific accumulation of mtDNA deletions was similar to CPEO patients and the worse rotarod performance of $Polg^{+/D257A}$ mice might be resulted from accumulation of mtDNA deletions. Thus, the $Polg^{+/D257A}$ mouse could be an animal model of adCPEO, in contrast with the $Polg^{D257A/D257A}$ mice that have the systemically premature-aging phenotype derived from excessive mtDNA alterations, including mtDNA depletion and point mutations.

Recently, Dai et al. showed that $Polg^{+/D257A}$ mice performed comparably in the rotarod test to control mice.[37] There are several possible explanations for this discrepancy: protocol of rotarod test, analysis methods, genetic back ground, and housing environment. These differences between the previous report and our study could lead to this apparent discrepancy. Among them, housing environment of mice might have impact on the motor dysfunction because mice were kept in cages with a running wheel. Exercise might have become load for muscles. In addition, the genetic background of mice seems to be different: we backcrossed $Polg^{+/D257A}$ mice into C57BL/6JJcl before a conventional behavioral test battery, whereas Dai and colleagues intercrossed $Polg^{+/D257A}$ mice in a colony. Clinical heterogeneity of features and different age of onset is observed among patients even within a family of adCPEO carrying an identical mutation in *POLG*.[8,10,11,18] This may also be explained by genetic background and environmental factors. We clearly demonstrated that aging is a critical determinant for accumulation of mtDNA deletions due to *Polg* mutation. However, other genetic or environmental risk factors associated with disease onset and progression remain unclear. The $Polg^{+/D257A}$ mouse will be useful for exploring and evaluating these risk factors.

There are two explanations for the tissue specificity of adCPEO symptoms due to a *POLG* mutation. First, the muscles and brain may show functional impairment at relatively low levels of mtDNA deletions, which does not cause dysfunction in other tissues. Second, the muscles and brain may accumulate more mtDNA deletions than other types of tissues. Our data suggest that the latter possibility is more likely as mtDNA deletions

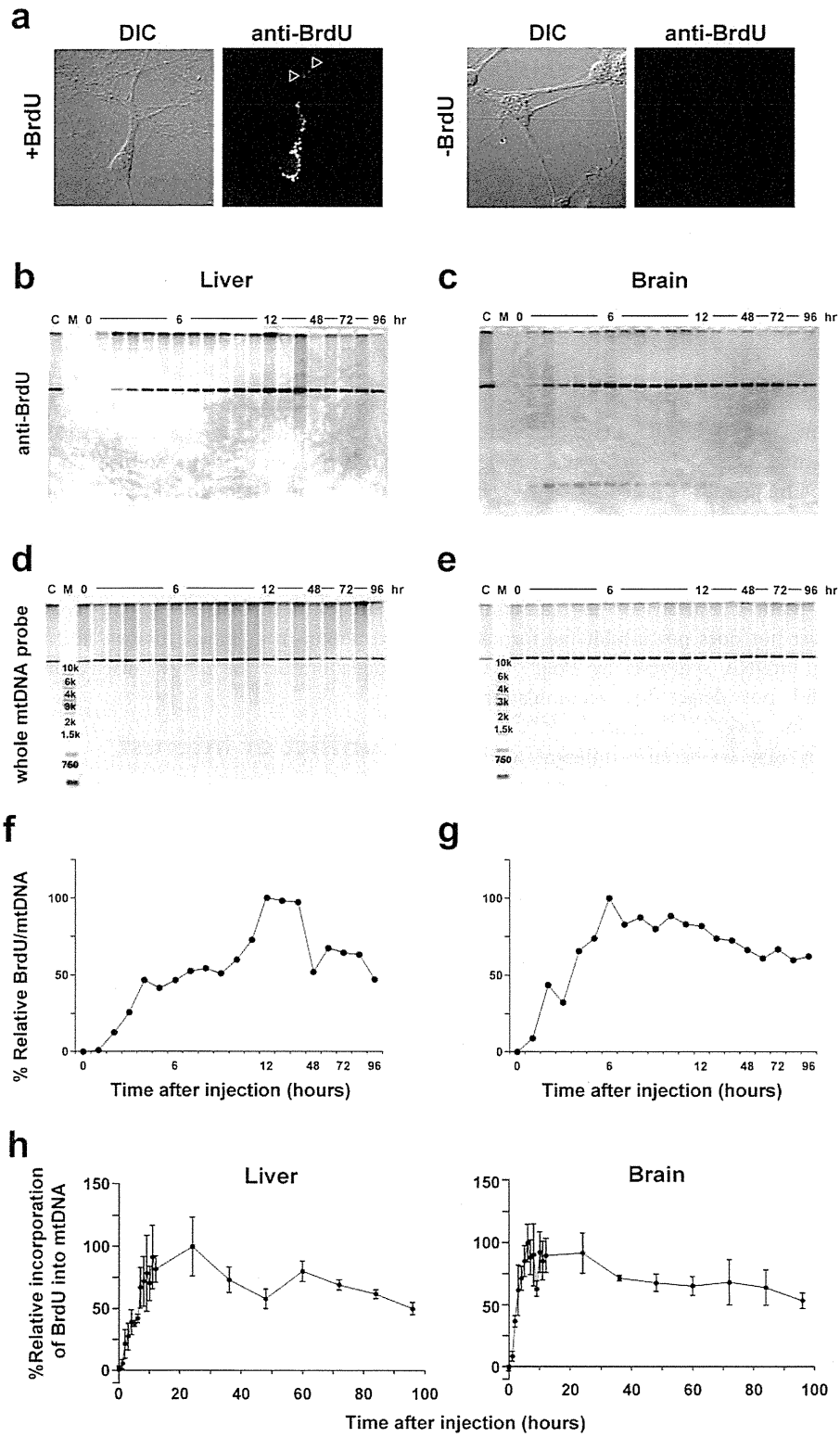

Figure 4. (A) Immunofluorescence analysis for the incorporation of BrdU in primary cultures of neurons prepared from mice at E17. After 9 days of culture, neurons exhibiting morphological differentiation with neurite elongations (left panels) were stained with an anti-BrdU antibody (right panels). Localization of BrdU was observed in the mitochondria of cell bodies and neurites (open arrow heads), but not in the nuclei of postmitotic neurons in the presence 10 μmol/L BrdU (lower panels), although no signal was observed in the absence of BrdU (upper panels). Assessment of newly generated mtDNA in the liver (B, D, and F) and brain (C, E, and G) using BrdU. Representative result is shown. (B and C) Southwestern blot analysis of purified mtDNA from the liver and posterior cortex after intraperitoneal injection of BrdU into adult mice. A control sample was applied to normalize the signals on each membrane (lane "C"). (D and E) Southern blot analysis using the same membrane from B and C. Analysis was performed from each injection independently ($n = 3$). (F and G) Quantification of incorporation of BrdU into mtDNA in the liver and cerebral cortex. The vertical axis represents the relative level of BrdU incorporation into mtDNA to the peak in each experiment. (H) Quantitative analysis of BrdU incorporation into mtDNA in the liver (upper graph) and cerebral cortex (lower graph). In ANCOVA in which a factor of tissue and a covariate of time was applied ($n = 3$, % mean ± SE), there was a significant effect of tissue ($P < 0.05$) and time ($P < 0.001$) as well as a significant interaction between region and time ($P < 0.03$). The time to reach the half of the maximum level of BrdU incorporation was shorter in the cerebral cortex (2–3 h) of the brain than in the liver (7–8 h).

preferentially accumulated in the muscles and brain in *Polg*$^{+/D257A}$ mice. mtDNA deletions may preferentially accumulate in the muscles and brain because myocytes and neurons are not frequently replaced by newly generated cells.

The results of the present study analyzing mtDNA in *Polg*$^{+/D257A}$ mice suggest that normal Polg in one allele is sufficient to repair point mutations or to maintain the mtDNA copy number but does not inhibit the formation of deletions during mtDNA synthesis by Polg^{D257A}.[38,39] Previous reports did not detect the accumulation of mtDNA deletions in *Polg*$^{+/D257A}$ mice.[22,23,26–29] This apparent discrepancy may be because different methods were used; Southern blot analysis with labeled whole mtDNA or a large variety of labeled oligonucleotides as a probe was used in previous studies, while the D-loop region that containing the replication origin for the heavy strand of mtDNA was used as a probe in this study. The presence of the D-loop in deleted mtDNAs suggests that the molecules are replicated and amplified, which explains why mtDNA deletions accumulate in an exponential manner along with aging. Indeed, D-loop retaining mtDNAs with deletions replicate more efficiently than full-length mtDNAs.[40] Therefore, higher activity of mtDNA synthesis in the brain may contribute at least in part to tissue-specific accumulation of mtDNA deletions. Further studies are needed to understand how mtDNAs containing deletions replicate through the action of normal or mutant Polg or both in the brain subregions of *Polg*$^{+/D257A}$ mice and to clarify how pathological accumulation of mtDNA deletions cause chronic progression of neuromuscular symptoms of CPEO.

Acknowledgments

This work was supported by grants from the Laboratory for Molecular Dynamics of Mental Disorders, RIKEN Brain Science Institute (BSI), a Grant-in-Aid from the Japanese Ministry of Health and Labor, and Grants-in-Aid from the Japanese Ministry of Education, Culture, Sports, Science and Technology. S. F. is supported by Grants-in-Aid for young scientists from the Japanese Ministry of Education, Culture, Sports, Science and Technology, and Grants-in-Aid for young scientists from Shiga University of Medical Science. We are grateful to the staff at the Divisions of Animal Experiments and Common Instrumentations in Research Resources Center, RIKEN BSI, for technical assistance, Yoko Nakano for DNA extraction from mouse tissues, and the other members in our laboratory for various discussions.

Conflict of Interest

Dr. Kato received honorarium for manuscripts, lectures, or consultancy from Kyowa Hakko Kirin Co., Ltd., Eli Lilly Japan K.K., Otsuka Pharmaceutical Co., Ltd., GlaxoSmithKline K.K., Taisho Toyama Pharmaceutical Co., Ltd., Dainippon Sumitomo Pharma Co., Ltd., Meiji Seika Pharma Co., Ltd., Pfizer Japan Inc., Mochida Pharmaceutical Co., Ltd., Shionogi & Co., Ltd., Janssen Pharmaceutical K.K. and Astellas Pharma Inc. , and grants from Takeda Pharmaceutical Co., Ltd. outside the submitted work. Dr. Prolla has a United States patent 7,126,040 and a founding owner and consultant for LifeGen Technologies, specializing in nutraceutical interventions in aging. Dr. Kujoth has a United States patent 7,126,040. Other authors declare no conflict of interest.

References

1. DiMauro S, Davidzon G. Mitochondrial DNA and disease. Ann Med 2005;37:222–232.
2. Wallace DC. Mitochondrial diseases in man and mouse. Science 1999;283:1482–1488.
3. Van Goethem G, Martin JJ, Van Broeckhoven C. Progressive external ophthalmoplegia characterized by multiple deletions of mitochondrial DNA: unraveling the pathogenesis of human mitochondrial DNA instability and the initiation of a genetic classification. Neuromolecular Med 2003;3:129–146.

4. Suomalainen A, Majander A, Haltia M, et al. Multiple deletions of mitochondrial DNA in several tissues of a patient with severe retarded depression and familial progressive external ophthalmoplegia. J Clin Invest 1992;90:61–66.
5. Melberg A, Arnell H, Dahl N, et al. Anticipation of autosomal dominant progressive external ophthalmoplegia with hypogonadism. Muscle Nerve 1996;19:1561–1569.
6. Suomalainen A, Majander A, Wallin M, et al. Autosomal dominant progressive external ophthalmoplegia with multiple deletions of mtDNA: clinical, biochemical, and molecular genetic features of the 10q-linked disease. Neurology 1997;48:1244–1253.
7. Moslemi AR, Melberg A, Holme E, Oldfors A. Autosomal dominant progressive external ophthalmoplegia: distribution of multiple mitochondrial DNA deletions. Neurology 1999;53:79–84.
8. Van Goethem G, Dermaut B, Lofgren A, et al. Mutation of *POLG* is associated with progressive external ophthalmoplegia characterized by mtDNA deletions. Nat Genet 2001;28:211–212.
9. Siciliano G, Tessa A, Petrini S, et al. Autosomal dominant external ophthalmoplegia and bipolar affective disorder associated with a mutation in the *ANT1* gene. Neuromuscul Disord 2003;13:162–165.
10. Luoma P, Melberg A, Rinne JO, et al. Parkinsonism, premature menopause, and mitochondrial DNA polymerase γ mutations: clinical and molecular genetic study. Lancet 2004;364:875–882.
11. Mancuso M, Filosto M, Bellan M, et al. *POLG* mutations causing ophthalmoplegia, sensorimotor polyneuropathy, ataxia, and deafness. Neurology 2004;62:316–318.
12. Kato T. Mitochondrial dysfunction as the molecular basis of bipolar disorder: therapeutic implications. CNS Drugs 2007;21:1–11.
13. Smits BW, Fermont J, Delnooz CC, et al. Disease impact in chronic progressive external ophthalmoplegia: more than meets the eye. Neuromuscul Disord 2011;21:272–278.
14. Stumpf JD, Copeland WC. Mitochondrial DNA replication and disease: insights from DNA polymerase γ mutations. Cell Mol Life Sci 2011;68:219–233.
15. Carrozzo R, Hirano M, Fromenty B, et al. Multiple mtDNA deletions features in autosomal dominant and recessive diseases suggest distinct pathogeneses. Neurology 1998;50:99–106.
16. Horvath R, Hudson G, Ferrari G, et al. Phenotypic spectrum associated with mutations of the mitochondrial polymerase gamma gene. Brain 2006;129:1674–1684.
17. Kollberg G, Jansson M, Pérez-Bercoff A, et al. Low frequency of mtDNA point mutations in patients with PEO associated with *POLG1* mutations. Eur J Hum Genet 2005;13:463–469.
18. Hudson G, Schaefer AM, Taylor RW, et al. Mutation of the linker region of the polymerase γ-1 (*POLG1*) gene associated with progressive external ophthalmoplegia and Parkinsonism. Arch Neurol 2007;64:553–557.
19. Suomalainen A, Kaukonen J. Diseases caused by nuclear genes affecting mtDNA stability. Am J Med Genet 2001;106:53–61.
20. Spelbrink JN, Li FY, Tiranti V, et al. Human mitochondrial DNA deletions associated with mutations in the gene encoding Twinkle, a phage T7 gene 4-like protein localized in mitochondria. Nat Genet 2001;28:223–231.
21. Longley MJ, Clark S, Yu Wai Man C, et al. Mutant *POLG2* disrupts DNA polymerase γ subunits and causes progressive external ophthalmoplegia. Am J Hum Genet 2006;78:1026–1034.
22. Trifunovic A, Wredenberg A, Falkenberg M, et al. Premature aging in mice expressing defective mitochondrial DNA polymerase. Nature 2004;429:417–423.
23. Kujoth GC, Hiona A, Pugh TD, et al. Mitochondrial DNA mutations, oxidative stress, and apoptosis in mammalian aging. Science 2005;309:481–484.
24. Edgar D, Shabalina I, Camara Y, et al. Random point mutations with major effects on protein-coding genes are the driving force behind premature aging in mtDNA mutator mice. Cell Metab 2009;10:131–138.
25. Hiona A, Sanz A, Kujoth GC, et al. Mitochondrial DNA mutations induce mitochondrial dysfunction, apoptosis and sarcopenia in skeletal muscle of mitochondrial DNA mutator mice. PLoS One 2010;5:e11468.
26. Williams SL, Huang J, Edwards YJ, et al. The mtDNA mutation spectrum of the progeroid Polg mutator mouse includes abundant control region multimers. Cell Metab 2010;12:675–682.
27. Ameur A, Stewart JB, Freyer C, et al. Ultra-deep sequencing of mouse mitochondrial DNA: mutational patterns and their origins. PLoS Genet 2011;7:e1002028.
28. Vermulst M, Bielas JH, Kujoth GC, et al. Mitochondrial point mutations do not limit the natural lifespan of mice. Nat Genet 2007;39:540–543.
29. Vermulst M, Wanagat J, Kujoth GC, et al. DNA deletions and clonal mutations drive premature aging in mitochondrial mutator mice. Nat Genet 2008;40:392–394.
30. Kraytsberg Y, Simon DK, Turnbull DM, et al. Do mtDNA deletions drive premature aging in mtDNA mutator mice? Aging Cell 2009;8:502–506.
31. Kasahara T, Kubota M, Miyauchi T, et al. Mice with neuron-specific accumulation of mitochondrial DNA mutations show mood disorder-like phenotypes. Mol Psychiatry 2006;11:577–593.
32. Fuke S, Kubota-Sakashita M, Kasahara T, et al. Regional variation in mitochondrial DNA copy number in mouse brain. Biochim Biophys Acta 2011;1807:270–274.

33. Battersby BJ, Shoubridge EA. Selection of a mtDNA sequence variant in hepatocytes of heteroplasmic mice is not due to differences in respiratory chain function or efficiency of replication. Hum Mol Genet 2001;10:2469–2479.
34. Hayashi A, Kasahara T, Iwamoto K, et al. The role of brain-derived neurotrophic factor (BDNF)-induced XBP1 splicing during brain development. J Biol Chem 2007;282:34525–34534.
35. Magnusson J, Orth M, Lestienne P, et al. Replication of mitochondrial DNA occurs throughout the mitochondria of cultured human cells. Exp Cell Res 2003;289:133–142.
36. Hitoshi S, Alexon T, Tropepe V, et al. Notch pathway molecules are essential for the maintenance, but not for the generation, of mammalian neural stem cells. Genes Dev 2002;16:846–858.
37. Dai Y, Kiselak T, Clark J, et al. Behavioral and metabolic characterization of heterozygous and homozygous POLG mutator mice. Mitochondrion 2013;13:282–291.
38. Bailey L, Cluett TJ, Reyes A, et al. Mice expressing an error-prone DNA polymerase in mitochondria display elevated replication pausing and chromosomal breakage at fragile sites of mitochondrial DNA. Nucleic Acid Res 2009;37:2327–2335.
39. Krishnan KJ, Reeve AK, Samuels DC, et al. What causes mitochondrial DNA deletions in human cells? Nat Genet 2008;40:275–279.
40. Diaz F, Bayona-Bafaluy MP, Rana M, et al. Human mitochondrial DNA with large deletions repopulates organelles faster than full-length genomes under relaxed copy number control. Nucleic Acids Res 2002;30:4626–4633.

Supporting Information

Additional Supporting Information may be found in the online version of this article:

Figure S1. Results of conventional behavioral test battery. Male mice at 34 weeks old were used for these analyses (mean ± SEM is shown in all graphs.). (A) Body weight. $Polg^{D257A/D257A}$ mice weighed less than $Polg^{+/D257A}$ and $Polg^{+/+}$ mice ($n = 10$, $^*P < 0.05$, one-way ANOVA followed by Tukey's HSD). (B) Open field test. Total distance traveled per 5 min is shown. There was a significant main effect of genotype ($P = 0.046$) and bin of time ($P = 0.00307$) in the GLM repeated measures ANOVA. A significant interaction between genotype and the bin was observed ($P = 1.01 \times 10^{-5}$). In analysis of each 5 min, the total distance of $Polg^{D257A/D257A}$ mice was shorter than for $Polg^{+/D257A}$ and $Polg^{+/+}$ mice ($n = 10$, $^*P < 0.05$, one-way ANOVA followed by Tukey's HSD). (C) A percentage of total time in center in an open field test. There was no significant difference among genotypes ($n = 10$, $P = 0.817$, one-way ANOVA). (D) Total distance traveled in elevated plus maze test. The total distance of $Polg^{D257A/D257A}$ mice was shorter than for $Polg^{+/D257A}$ and $Polg^{+/+}$ mice ($n = 10$, $^*P < 0.05$, one-way ANOVA followed by Tukey's HSD). (E) A percentage of total time in the open arm of the elevated plus maze. There was no significant difference among genotypes ($n = 10$, $P = 0.142$, Kruskal–Wallis test). (F) A percentage of number of entries into the open arm in the elevated plus maze test. There was no significant difference among genotypes ($n = 10$, $P = 0.066$, one-way ANOVA). (G) Y-maze test. Numbers of entries into the arm are shown. $Polg^{D257A/D257A}$ mice showed fewer entries than $Polg^{+/D257A}$ and $Polg^{+/+}$ mice ($n > 9$, $^*P < 0.05$, one-way ANOVA followed by Tukey's HSD). The low number of entries of $Polg^{D257A/D257A}$ mice (2.3 ± 0.65) was seemingly due to a lack of spontaneous behavior. Thus, the number of alternations does not make sense in the $Polg^{D257A/D257A}$ mice. No difference was found in the alternation task between $Polg^{+/D257A}$ and $Polg^{+/+}$ mice ($n = 8$, $P = 0.618$, *t*-test). (H) Prepulse inhibition (PPI) test. Effect of prepulse on the auditory startle response was examined. There was a significant main effect of prepulse ($P = 7.74 \times 10^{-9}$) but not genotype ($P = 0.171$) with the GLM repeated measures ANOVA. There was no significant interaction between PPI and genotype ($P = 0.469$). (I) Passive avoidance test. The genotypes did not differ in time until entry into the black box in both training ($P = 0.913$, Kruskal–Wallis test) and the test ($P = 0.795$, Kruskal–Wallis test).

Figure S2. Methodology for analysis of accumulation of multiple mtDNA deletions. (A) Southern blot analysis of total mtDNA from frontal lobe using the same membrane as Figure 2C with a probe for cytochrome c oxidase subunit I (*COX1*) gene (left panel), for nicotinamide adenine dinucleotide dehydrogenase subunit 4 (*ND4*) genes (middle panel), or for whole mtDNA (right panel). Even in $Polg^{D257A/D257A}$ mice, there was no detectable signal other than full-length mtDNA. (B) For a quantitative real-time PCR (qPCR) analysis for the statistical comparison of the relative accumulation of mtDNA deletions, typical standard curves of serially diluted control mtDNA, which was extracted from the frontal lobe of aged $Polg^{D257A/D257A}$ mice and contains mtDNA deletions, as measured by qPCR analysis. Each circle indicates a single measurement ($n = 4$). Significantly high linearity in this range for the standard samples was assured in each PCR plate ($R^2 > 0.95$). (C) Agarose gel electrophoresis analysis and identification of amplifications of multiple mtDNA deletions after real-time PCR. A dilution series of control mtDNA for a standard curve, mtDNA of the frontal lobe

of $Polg^{+/+}$ and $Polg^{+/D257A}$ mice are shown. No amplification was detected without mtDNA (lane N).

Figure S3. Western blot analysis for levels of the respiratory chain enzyme complex subunits in the frontal lobes of $Polg^{+/+}$ and $Polg^{+/D257A}$ mice at 96 weeks of age. (A) Subunits of mitochondrial complex are shown as follows: complex I subunit Ndufb8 (CI), complex II subunit Sdhb (CII), complex III subunit Uqcrc2 (CIII), complex IV subunit mt-Co1 (CIV), and complex V subunit Atp5a1 (CV) (upper panel). β-actin was detected as a loading control in the same membrane after stripping antibodies (lower panel). (B) Densitometric quantification of the ratios of each mitochondrial complex subunit/β-actin immunoblot levels in Western blot analysis ($n = 6$, mean ± SE, $*P < 0.05$, *t*-test). One of mtDNA-encoded subunits of respiratory complex, mt-Co1, showed a significant decrease in protein level.

Figure S4. Tissue distribution of accumulation of mtDNA deletions in $Polg^{+/+}$ mice at 48 weeks ($n = 3$), $Polg^{+/D257A}$ and $Polg^{D257A/D257A}$ mice at 24 weeks ($n = 4$). The qPCR analysis was applied to mtDNAs extracted from five areas of the brain (frontal lobe [Fl], posterior cortices [Cx], hippocampus [Hp], basal ganglia [Bg], and cerebellum [Cb]) and four somatic tissues (heart, liver [Liv], kidney [Kid], and skeletal muscle [Sk]). The vertical axis represents the relative value normalized to the average level of deletions in the frontal lobe of $Polg^{+/+}$ mice ($*P < 0.05$, $**P < 0.01$, mean ± SD, Welch ANOVA followed by the Dunnett T3 test). In all areas and tissues, $Polg^{D257A/D257A}$ mice showed significantly higher accumulation of mtDNA deletions than did the other mice. In both $Polg^{D257A/D257A}$ and $Polg^{+/D257A}$ mice ($P < 0.0001$), but not in $Polg^{+/+}$ mice ($P = 0.332$), a significant tissue-dependent variation in the level of the accumulation was found by Welch ANOVA. A multiple comparison by the Dunnett T3 test showed a significant tissue-dependent difference in accumulation in $Polg^{D257A/D257A}$ and $Polg^{+/D257A}$ mice, as follows. In $Polg^{D257A/D257A}$ mice: Fl, Cx, and heart > Cb, Liv, and Sk; Hp and Bg > Liv and Sk; Fl > Bg ($P < 0.05$). In $Polg^{+/D257A}$ mice: Fl and heart > Liv, Kid, and Sk; Fl > Bg and Cb ($P < 0.05$).

Figure S5. Analysis of age-dependent accumulation of mtDNA deletions in posterior cortices, hippocampus, basal ganglia, cerebellum, and heart of $Polg^{+/D257A}$ and $Polg^{+/+}$ mice at 12, 24, 48, 60, 72, 84, 101 weeks using qPCR. Values are represented relative to the average of 12-week-old $Polg^{+/+}$ mice in each tissue. Each circle indicates one mouse ($n = 4$; two males and two females). Significant differences were detected at several ages except for liver ($*P < 0.05$). Statistical analysis results including the frontal lobe and skeletal muscles are described in Figure 3C.

Figure S6. Effect of age, tissue, and genotype on mtDNA copy number, as measured by qPCR from total DNA. The mtDNA copy number was measured in eight regions: frontal lobe, other cortices, hippocampus, basal ganglia, cerebellum, heart, liver, and skeletal muscle. The copy number per cell was measured by qPCR for the D-loop of mtDNA using the *ApoB* gene as a reference for nuclear genome copy number. The vertical axis represents the relative value normalized to each ratio in the frontal lobe of $Polg^{+/+}$ mice ($n = 4$, mean ± SD). The horizontal axis represents the age. A significant difference was found in mtDNA copy number among tissues ($P < 1.0 \times 10^{-10}$, ANCOVA), whereas age and genotype showed no significant effect ($P > 0.05$).

Figure S7. Analysis of region-dependent accumulation of mtDNA deletions in skeletal muscles from hind limbs of $Polg^{+/D257A}$ and $Polg^{+/+}$ mice at 37 weeks using qPCR. Values are represented relative accumulation of mtDNA deletions to that in the thigh of $Polg^{+/+}$ mice. Each circle indicates one mouse ($n = 5$; two males and three females), and each horizontal bar show the mean value. Significant differences were detected only in posterior crus ($*P < 0.01$, Mann–Whitney *U* test).

Figure S8. Analysis of complex IV (COX) enzyme activity in skeletal muscles of male $Polg^{+/D257A}$ and $Polg^{+/+}$ mice at 96 weeks of age ($n = 6$, mean ± SE). The vertical axis represents absorbance at 550 nm (A) or the relative activities normalized to the average value of activities in $Polg^{+/+}$ mice (B). There was a significant decrease in COX activities in skeletal muscles of $Polg^{+/D257A}$ mice ($*P < 0.01$, *t*-test).

Figure S9. Southern blot analysis of mtDNA in neural stem cell (NSC) cultured for 5 weeks from the mouse embryo at gestational day 14.5 ($Polg^{+/+}$ mice: $n = 2$, $Polg^{+/D257A}$ mice: $n = 3$, $Polg^{D257A/D257A}$ mice: $n = 3$) and 16.5 ($Polg^{+/+}$ mice: $n = 2$, $Polg^{+/D257A}$ mice: $n = 2$). NSC from $Polg^{D257A/D257A}$ mice at E14.5 accumulated mtDNA deletions. However, there was no detectable signal other than full-length mtDNA both in NSC from $Polg^{+/D257A}$ mice and that from $Polg^{+/+}$ mice.

Table S1. PCR primers.

Data S1. Supplementary methods.

nature COMMUNICATIONS

ARTICLE

Received 25 Feb 2014 | Accepted 16 Apr 2014 | Published 4 Jun 2014

DOI: 10.1038/ncomms4917

The FAM3 superfamily member ILEI ameliorates Alzheimer's disease-like pathology by destabilizing the penultimate amyloid-β precursor

Hiroshi Hasegawa[1,*,†], Lei Liu[1,*], Ikuo Tooyama[1], Shigeo Murayama[2] & Masaki Nishimura[1]

Accumulation of amyloid-β peptide (Aβ) in the brain underlies the pathogenesis of Alzheimer's disease (AD). Aβ is produced by β- and γ-secretase-mediated sequential proteolysis of amyloid-β precursor protein (APP). Here we identify a secretory protein named interleukin-like epithelial-mesenchymal transition inducer (ILEI, also known as FAM3 superfamily member C) as a negative regulator of Aβ production. ILEI destabilizes the β-secretase-cleaved APP carboxy-terminal fragment, the penultimate precursor of Aβ, by binding to the γ-secretase complex and interfering with its chaperone properties. Notch signalling and γ-secretase activity are not affected by ILEI. We also show neuronal expression of ILEI and its induction by transforming growth factor-β signalling. The level of secreted ILEI is markedly decreased in the brains of AD patients. Transgenic (Tg) overexpression of ILEI significantly reduces the brain Aβ burden and ameliorates the memory deficit in AD model mice. ILEI may be a plausible target for the development of disease-modifying therapies.

[1] Molecular Neuroscience Research Center, Shiga University of Medical Science, Seta-Tsukinowa, Otsu, Shiga 520-2192, Japan. [2] Department of Neuropathology, Tokyo Metropolitan Institute of Gerontology, Tokyo 173-0015, Japan. * These authors contributed equally to this work. † Present address: Minami-Kyoto Hospital, Kyoto, Japan. Correspondence and requests for materials should be addressed to M.N. (e-mail: mnishimu@belle.shiga-med.ac.jp).

The amyloid-β peptide (Aβ) is produced in neurons by two-step proteolytic processing of the amyloid-β precursor protein (APP)[1]. Ectodomain shedding by β-secretase, which is known as β-site APP-cleaving enzyme 1 (BACE1), yields the membrane-spanning carboxy-terminal fragment (CTF)-β. The aspartyl protease γ-secretase complex, which primarily comprises presenilin, nicastrin (NCT), anterior pharynx defective-1 (APH-1) and presenilin enhancer-2 (PEN-2), sequentially catalyses intramembrane proteolysis of APP-CTFβ, resulting in secretion of Aβ and liberation of the APP intracellular domain[1]. Each proteolysed derivative exhibits distinct physiological activities[2], and genetic ablation of APP in mice causes neurological deficits such as impairment of spatial learning and reduction in brain weight, which can be completely rescued by expression of the secreted ectodomain[3]. Ablation of the γ-secretase complex by genetic deletion of any of the core components causes early developmental defects that resemble a Notch phenotype, which is expected because γ-secretase is involved in transmembrane signal transduction by cleaving various membrane-spanning substrates, including Notch receptors[1].

A persistent imbalance between production and clearance of Aβ results in gradual accumulation of soluble and aggregated Aβ in the extracellular space of the brain parenchyma, which underlies the development of Alzheimer's disease (AD). Genetic mutations in APP, presenilin-1 (PS1) and presenilin-2 (PS2) modify Aβ biosynthesis and cause an autosomal dominant form of AD[4]. In contrast, alteration in Aβ metabolism in the common sporadic form of AD has not been fully clarified. However, an increase in the amount and activity of BACE1 and/or a decline in protein degradation capacity have been proposed as the primary events in the pathogenesis of sporadic AD[5–8]. In addition to Aβ, accumulation of APP-CTFs, which are sometimes associated with sporadic AD, may cause neurodegeneration by inducing abnormal membrane currents, decreased numbers of dendritic spines, neuronal cell death and inflammatory reactions[9,10].

Reduction in brain Aβ is the pivotal goal of disease-modifying therapy for AD. Although γ-secretase is a major target for therapeutic intervention, non-selective inhibition of its activity causes serious adverse effects due to blockade of Notch signalling and accumulation of neurotoxic APP-CTFs[1,11–13]. To avoid these adverse effects, finding novel approaches to negatively modulate Aβ generation is imperative. Several endogenous proteins interact with the γ-secretase complex and influence the efficacy of γ-secretase cleavage in distinct ways, including alteration of specific activities, substrate selectivity and assembly or subcellular localization of γ-secretase complexes[14–17].

In this study, we searched for additional proteins that affect Aβ generation by interacting with the γ-secretase complex. To date, multiple γ-secretase-modulating proteins have been identified by purification of intact γ-secretase complexes via affinity-mediated isolation of the major catalytic component, PS1 (refs 18,19), which is also involved in cellular Ca homeostasis, apoptosis and protein trafficking by binding additional or alternative partners[14]. In contrast, PEN-2 is exclusively involved in formation of the γ-secretase complex, as the cellular accumulation of PEN-2 is entirely dependent on the expression of the other core components. In addition, PEN-2 is the last component to be incorporated into the γ-secretase complex, and activated complexes exclusively contain PEN-2. Here, using PEN-2 affinity-mediated isolation of the γ-secretase complex, we identify a unique secretory protein that reduces cellular Aβ generation without inhibiting γ-secretase activity or Notch cleavage.

Results

ILEI is a γ-secretase complex-binding protein. We employed tandem affinity-tag purification (TAP)[20] to isolate the γ-secretase complex using PEN-2 as the bait, combined with stable silencing of endogenous PEN-2 expression. The abundance and stoichiometry of γ-secretase components are tightly regulated. Although exogenous PEN-2 can be incorporated into the γ-secretase complex by replacing endogenous PEN-2, high PEN-2 overexpression is required for sufficient replacement. To circumvent this problem, we first prepared PEN-2-knockdown HEK293 cell lines in which small interference RNA (siRNA) for PEN-2 was stably expressed. We chose a PEN-2-knockdown cell line that exhibited the lowest levels of PEN-2 expression and Aβ secretion. We then transfected this cell line with siRNA-resistant PEN-2 (srPEN-2) fused with a TAP tag (TAP-srPEN-2) and selected a cell line, referred to as HEK-TAP-PEN-2, which stably expressed TAP-srPEN-2 at a level equivalent to that of endogenous PEN-2. We confirmed that TAP-srPEN-2 was incorporated into the active γ-secretase complex and restored Aβ secretion (Supplementary Fig. 1).

The activity and composition of γ-secretase complexes are sensitive to several detergents but are only slightly affected by 1% 3-[(3-cholamidopropyl)dimethylammonio]-2-hydroxy-1-propanesulfonic acid (CHAPSO)[21]. We prepared CHAPSO lysates of HEK-TAP-PEN-2 cells and performed sequential isolation of TAP-srPEN-2-associated complexes. To distinguish non-specific binding proteins from proteins of interest, we used TAP-tag-transfected PEN-2-knockdown HEK293 (HEK-TAP-empty) cells as a control. Complexes isolated in two independent trials exhibited a similar pattern of banding on SYPRO- and silver-stained SDS–polyacrylamide gel electrophoresis (SDS–PAGE) gels (Fig. 1a). Proteins in each excised gel piece were digested with trypsin and subjected to liquid chromatography-tandem mass spectrometric analysis followed by a search of the Mascot database. Hits included the four core components and some known binding proteins of the γ-secretase complex. One of the identified peptides matched residues 164–179 of a 27-kDa protein referred to as interleukin-like epithelial-mesenchymal transition inducer (ILEI) or family with sequence similarity 3, member C (FAM3C) (NCBI Protein Database accession code NP_055703).

ILEI, which was originally identified in a database search for four-helix-bundle cytokines, is an evolutionarily conserved secretory protein[22]. ILEI is posttranslationally liberated from the membrane in secretory vesicles by cleavage of the signal sequence of the full-length (FL) precursor protein. Immunoblotting with an affinity-purified rabbit polyclonal anti-ILEI antibody revealed specific bands of 24 and 27 kDa in the conditioned medium and cell lysate of HEK293 cells, respectively, suggesting that the smaller species corresponded to a processed, secreted form of ILEI (Fig. 1b). Co-immunoprecipitation using native HEK293 cells indicated that antibodies against PS1, NCT, PEN-2 or APH-1 co-precipitated the precursor and processed forms of ILEI (Fig. 1b). The reverse assay revealed that the anti-ILEI antibody co-precipitated the four core components of the γ-secretase complex (Fig. 1c). Protein complex analysis using two-dimensional Blue Native SDS–PAGE suggested that ILEI is incorporated into multiple complexes of various molecular masses, one of which is comparable to that of the mature γ-secretase complex (Fig. 1d). These data confirmed the interaction between ILEI and the γ-secretase complex.

To determine the partner that directly interacts with endogenous ILEI, we treated HEK293 cells *in situ* with a thiol-cleavable, membrane-permeable, chemical crosslinker. The cells were then lysed in a Nonidet P-40 buffer to dissociate non-crosslinked components of the γ-secretase complex. In this lysate, monomeric components of the γ-secretase complex were reduced

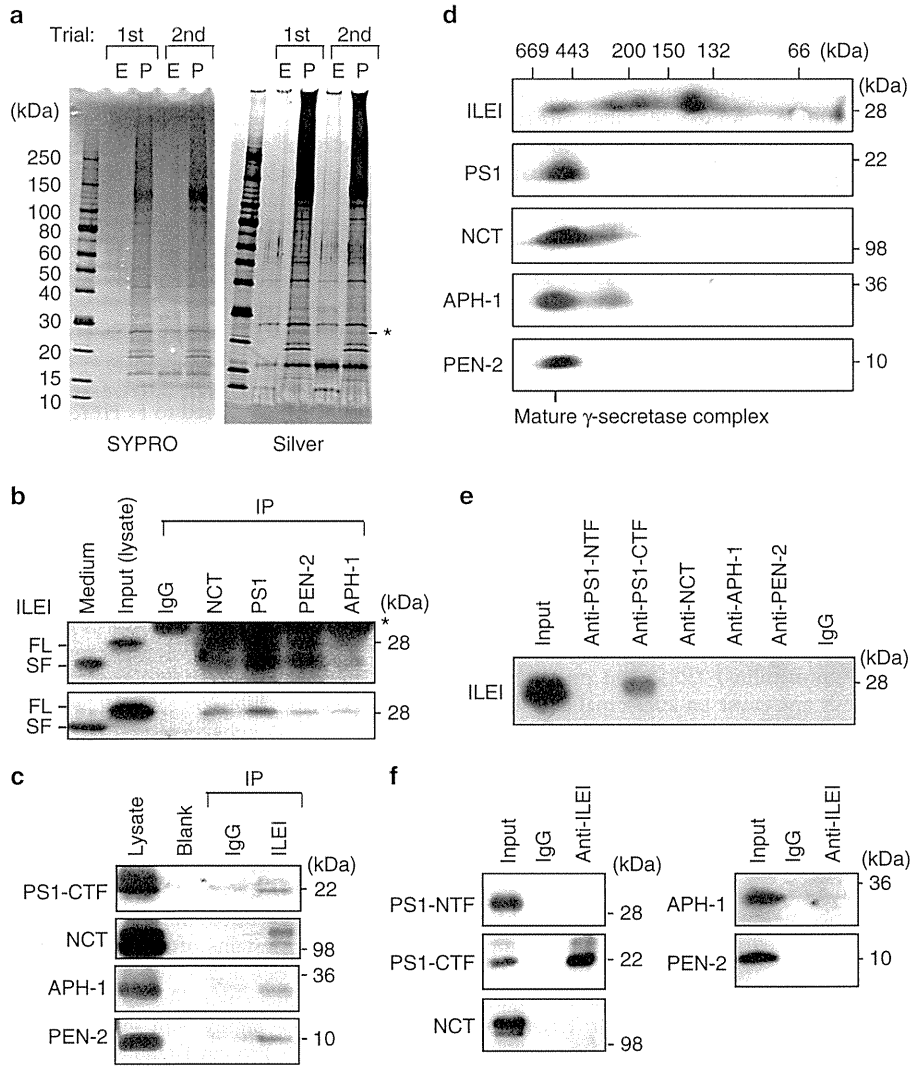

Figure 1 | ILEI is associated with mature γ-secretase complexes. (**a**) SYPRO- and silver-stained SDS-PAGE gels of TAP-tagged PEN-2-associated proteins isolated from lysates of HEK-TAP-PEN-2 (P) and HEK-TAP-empty (E) cells. ILEI was identified in the band indicated by the star. (**b**) Co-immunoprecipitation of endogenous ILEI and γ-secretase components. Native HEK293 cell lysates were immunoprecipitated with normal IgG or an antibody against NCT, PS1, PEN-2 or APH-1. The blot was probed with anti-ILEI antibody (upper panel). As the FL ILEI bands were close to the IgG light-chain bands, nanocapsules incorporating IgG Fc-binding Z domains were used instead of the secondary antibody for detection (lower panel). The star indicates the IgG band. FL, full-length; SF, secreted form. (**c**) Reverse co-immunoprecipitation. HEK293 cell lysates were precipitated using normal rabbit IgG (IP-IgG) or anti-ILEI antibody (IP-ILEI). The blots were probed using the indicated antibodies. (**d**) Two-dimensional Blue Native (BN)/SDS-PAGE analysis of ILEI and γ-secretase components. The membrane fraction of native HEK293 cells was subjected to two-dimensional BN/SDS-PAGE before immunoblotting. (**e**) Chemical crosslinking of ILEI with γ-secretase components. HEK293 cells were crosslinked *in situ* with dithiobis succinimidyl propionate. The 1% Nonidet P-40-solubilized cell lysate was subjected to immunoprecipitation. A blot of the immunoprecipitates with antibodies against the indicated proteins or normal IgG was probed with anti-ILEI antibody. (**f**) The crosslinked cell lysates were immunoprecipitated using normal IgG or anti-ILEI antibody. The blots were probed using the indicated antibodies.

by >80% on immunoblotting. PS1-CTF but not the other components co-immunoprecipitated ILEI (Fig. 1e). Conversely, the ILEI immunoprecipitates contained PS1-CTF but the other components were not present or were only faintly observed (Fig. 1f). These results suggest that ILEI directly binds to PS1-CTF.

ILEI reduces Aβ generation by destabilizing APP-CTFβ. RNA interference (RNAi)-mediated knockdown of endogenous ILEI in native HEK293 cells resulted in an approximately two-fold increase in Aβ40 and Aβ42 levels in the conditioned medium (Fig. 2a). Conversely, overexpression of ILEI decreased Aβ secretion (Fig. 2b). No significant alteration in the ratio of Aβ40 to Aβ42 was observed. ILEI knockdown or overexpression also increased or decreased APP intracellular domain generation, respectively (Fig. 2c).

We next determined whether ILEI affects γ-secretase cleavage of the Notch-1 receptor. Treatment with EDTA enhances the site-2 cleavage of transmembrane/intracellular Notch to generate Notch extracellular truncation, which is then directly cleaved by γ-secretase to release Notch intracellular domain[23]. ILEI

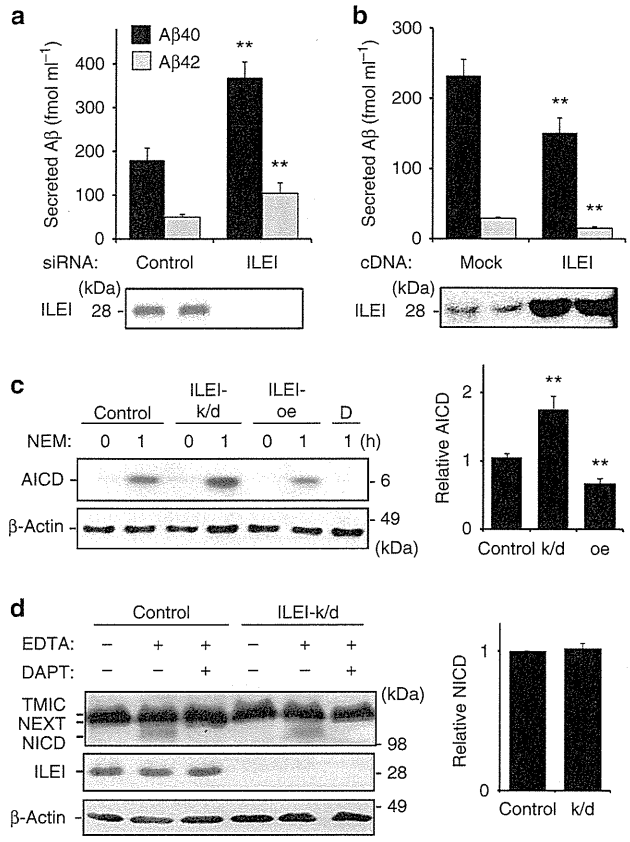

Figure 2 | ILEI inhibits cellular γ-secretase cleavage of APP but not Notch. Non-targeting control or ILEI-specific siRNA (**a**), or mock or ILEI cDNA (**b**) was transiently transfected into HEK293 cells. Aβ40 (black bars) and Aβ42 (grey bars) in the conditioned medium were measured using ELISA assays ($n=6$, mean ± s.d.). $^{**}P<0.01$ versus the control or the mock by Student's *t*-test. Lower panels show immunoblots of ILEI. (**c**) Immunoblot for APP intracellular domain (AICD) in control, ILEI-knockdown (k/d) or ILEI-overexpressing (oe) HEK293 cells. Cells were treated with 200 μM *N*-ethylmaleimide (NEM) for 1 h to block degradation of AICD[60]. AICD production was inhibited by DAPT (*N*-[*N*-(3,5-difluorophenacetyl)-L-alanyl]-*S*-phenylglycine *t*-butyl ester; 1 μM) treatment (**d**). The graph shows the relative intensity of AICD normalized to β-actin ($n=3$, mean ± s.d.). $^{**}P<0.01$ versus the control by Student's *t*-test. (**d**) Proteolysed derivatives of endogenous Notch-1 in control and ILEI-knockdown (k/d) mouse embryonic fibroblasts (MEFs). EDTA (1.5 mM) treatment induced cleavage of transmembrane/intracellular Notch (TMIC) to generate Notch extracellular truncation (NEXT), which was then cleaved by γ-secretase to release Notch intracellular domain (NICD). NICD production was inhibited by DAPT (1 μM) treatment. The graph shows the relative intensity of NICD normalized to β-actin ($n=3$, mean ± s.d.). No significant difference versus the control was found ($P>0.05$ by Student's *t*-test).

knockdown in mouse embryonic fibroblasts did not alter Notch intracellular domain generation from endogenous Notch in the presence of EDTA (Fig. 2d). In addition, we used a cell-based luciferase reporter assay for γ-secretase cleavage of Notch. The specificity was confirmed by treatment with a potent γ-secretase inhibitor, DAPT (*N*-[*N*-(3,5-difluorophenacetyl)-L-alanyl]-*S*-phenylglycine *t*-butyl ester), which attenuated luminescence (35.9 ± 4.5% of vehicle; vehicle, 100.0 ± 6.5%; $n=5$, $P=0.000$). Induction of luciferase activity was unaffected by transfection with ILEI siRNA (94.5 ± 12.5% of control; control, 100.0 ± 5.7%; $n=5$, $P=0.449$) or ILEI complementary DNA (96.8 ± 8.9% of mock; mock, 100.0 ± 8.2%; $n=5$, $P=0.596$). Thus, ILEI does not perturb γ-secretase processing of Notch.

To test whether ILEI directly inhibits γ-secretase activity, we evaluated Aβ generation in a cell-free assay in which microsome fractions derived from HEK293 cells treated with non-targeting control or ILEI-specific siRNA were incubated with excess recombinant APP-CTFβ. Unexpectedly, we found no significant difference in Aβ generation ($n=6$, $P=0.851$ for Aβ40; $P=0.561$ for Aβ42) between control (Aβ40: 3,253.3 ± 399.0, Aβ42: 597.7 ± 23.8 fmol ml^{-1}) and ILEI-knockdown cells (Aβ40: 3,181.9 ± 306.4, Aβ42: 614.5 ± 28.9 fmol ml^{-1}), indicating that ILEI reduces cellular Aβ generation without inhibiting γ-secretase activity. This result and the observation that ILEI was processed normally in the presence of DAPT (Supplementary Fig. 2a) further suggest that ILEI is not a competitive substrate of γ-secretase. In addition, ILEI knockdown did not detectably affect the cellular expression levels or subcellular localization of γ-secretase components, the intracellular trafficking of APP, or the Aβ secretion process (Supplementary Figs 2b-d and 3a). We also excluded the possibility that ILEI accelerated degradation of secreted Aβ in the culture medium (Supplementary Fig. 3b).

Accordingly, ILEI knockdown increased the level of cellular APP-CTFs (APP-CTFα and APP-CTFβ) without augmenting APP-FL or secreted ectodomains of APP (Fig. 3a). ILEI knockdown did not change APP transcript expression as measured with quantitative real-time PCR (104.1 ± 3.8% of control; control, 100.0 ± 2.9%; $n=3$, $P=0.291$) or cellular β-secretase activity as measured with an *in vitro* assay (104.4 ± 7.31% of control; control, 100.0 ± 6.1%; $n=3$, $P=0.555$). We thus reasoned that ILEI knockdown stabilizes APP-CTFβ to increase Aβ generation. A cycloheximide chase assay indicated that ILEI knockdown significantly extended the half-life of APP-CTFs but not APP-FL (Fig. 3b). Altered ILEI expression levels did not change the levels of Beclin-1 or Rab5a or the subcellular localization of APP-CTFs (Supplementary Fig. 3a and c), suggesting that stabilization of APP-CTFs is not mediated by inactivation of general protein degradation through lysosomal/autophagosomal pathways or a defect in APP-CTF trafficking. The effect of ILEI knockdown on APP metabolism could be rescued by transfection of siRNA-resistant ILEI cDNA (Fig. 3c), ruling out potential off-target effects of the siRNA-mediated RNAi.

We examined whether ILEI also acts on low-density lipoprotein receptor-related protein 1 (LRP1) and N-cadherin, which are other substrates of γ-secretase. Knockdown or overexpression of ILEI did not affect accumulated levels of LRP1 or N-cadherin CTFs (Fig. 3d). Taken together with the results for Notch-1 (Fig. 2d), our results suggest that ILEI exhibits selectivity for APP-CTFs.

ILEI interferes with the APP-CTF-stabilizing property of PS1. Processed ILEI is secreted from the cell, whereas intracellular ILEI is mostly associated with the microsome fraction (Supplementary Fig. 4a). Hence, we next determined whether extracellular application of a secreted form of ILEI decreased cellular Aβ secretion. We purified a recombinant polypeptide of processed ILEI from the conditioned medium of C-terminally V5-His-tagged ILEI (ILEI-VH)-overexpressing HEK293 cells (Supplementary Fig. 4b). When added into the culture medium of ILEI-knockdown HEK293 cells, purified ILEI-VH suppressed the levels of secreted Aβ and cellular APP-CTFs in a dose-dependent manner (Fig. 4a). Purified ILEI-VH was detected in perinuclear vesicular compartments and was associated with PS1 (Fig. 4b,c). These results suggest that ILEI acts on the extracellular side of the cell membrane and is endocytosed into the cell. In contrast, when we added purified ILEI-VH to cell-free mixtures and performed

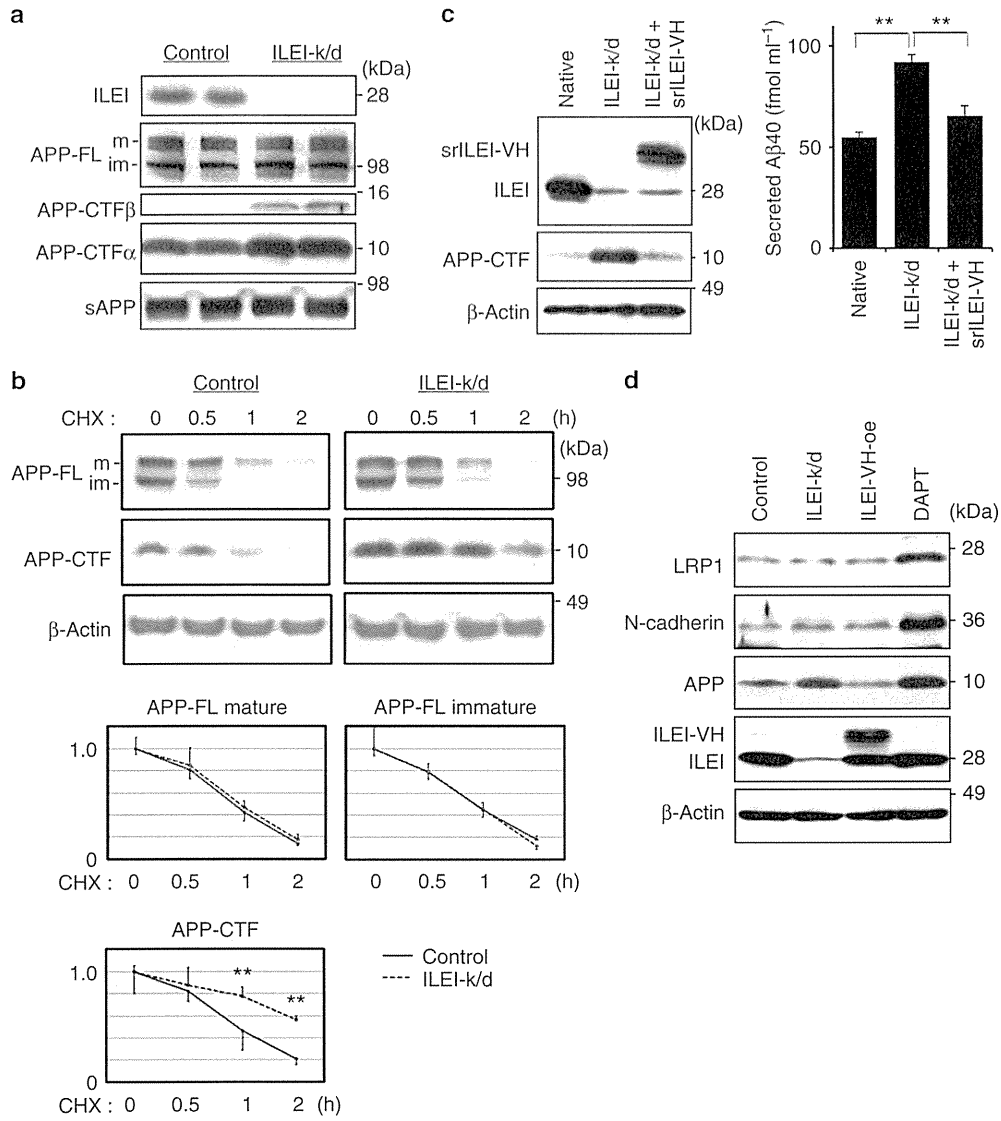

Figure 3 | ILEI knockdown selectively stabilizes APP-CTFs. (**a**) Immunoblots for APP and its proteolysed derivatives in control and ILEI-knockdown (k/d) HEK293 cells. The same amount of protein from cell lysates (for ILEI, APP FL and APP-CTFs) or conditioned medium (for secreted ectodomain; sAPP) was loaded. For APP-CTFβ, a longer exposure image is shown. m, mature; im, immature. (**b**) Immunoblots of APP-FL and APP-CTF in a cycloheximide (CHX) chase assay. m, mature; im, immature. Non-targeting control or ILEI-specific siRNA-transfected HEK293 cells were treated with 50 μg ml^{-1} CHX for the indicated times. β-Actin was used as a loading control. The graphs below show the relative intensity of the bands ($n=5$, mean ± s.d.). $^{**}P<0.01$ versus the control by Student's *t*-test. (**c**) The restoring effect of siRNA-resistant ILEI-V5-His (srILEI-VH) on the levels of APP-CTFs and secreted Aβ. ILEI-specific siRNA-transfected HEK293 cells were further transfected with srILEI-VH. APP-CTF was analysed with immunoblotting, and secreted Aβ40 was measured with ELISA ($n=3$, mean ± s.d.). $^{**}P<0.01$ by Student's *t*-test. (**d**) Immunoblots for LRP1-CTF (25 kDa), N-cadherin-CTF (36 kDa) and APP-CTF (10 kDa) in control, stable ILEI-knockdown (k/d), stable ILEI-VH-overexpressing (oe) and DAPT (*N*-[*N*-(3,5-difluorophenacetyl)-L-alanyl]-*S*-phenylglycine *t*-butyl ester; 1 μM)-treated HEK293 cells. β-Actin was used as a loading control.

γ-secretase assays using microsome fractions derived from ILEI-knockdown HEK293 cells, Aβ generation was not altered (Supplementary Fig. 4c).

Although we identified ILEI as a γ-secretase complex-binding protein, whether ILEI interaction with the γ-secretase complex mediated the stabilization of APP-CTFs was not clear. To address this issue, we tested the effect of ILEI knockdown on APP-CTF levels in PS1/PS2-knockdown HEK293 cells. High levels of APP-CTFs accumulated in PS1/PS2-knockdown cells in which the γ-secretase complex was ablated. ILEI knockdown did not lead to any further increase in APP-CTFs (Fig. 4d). In contrast, as shown in Fig. 4d, the APP-CTF level was increased by ILEI knockdown in PEN-2-knockdown HEK293 cells, which exclusively contained immature, inactive γ-secretase complexes[24]. Furthermore, ILEI knockdown and ILEI-VH treatment enhanced and reduced accumulation of APP-CTFs in the presence of a γ-secretase inhibitor, respectively (Fig. 4a,d). Thus, ILEI requires interaction with the γ-secretase complex, regardless of whether the complex is enzymatically active or inactive, to alter the stability of APP-CTFs. In contrast, co-immunoprecipitation assays revealed no direct interaction between ILEI and APP-CTFs (Supplementary Fig. 3d).

We next asked whether ILEI competes with APP-CTFs for binding with the γ-secretase complex. Co-immunoprecipitation

assays indicated that the amount of PS1-bound APP-CTFs was inversely correlated with the ILEI expression level (Fig. 4e). In contrast, alternative co-immunoprecipitation assays suggested that the expression level of APP did not influence the amount of PS1-bound ILEI (Fig. 4f). These results imply that ILEI non-competitively interferes with the binding between the γ-secretase complex and APP-CTFs.

The PS1/γ-secretase complex stably binds APP-CTFs and protects them from non-specific degradation[21,25]. Analysis of the APP-CTF-stabilizing property is hampered by γ-secretase